Chemical pattern formation induced by a shear flow in a two-layer model

Desiderio A. Vasquez*
Departamento de Ciencias, Sección Física, Pontificia Universidad Católica del Perú, Apartado 1761, Lima, Peru

Jeff Meyer and Hans Suedhoff
Department of Physics, Indiana University Purdue University Fort Wayne, Fort Wayne, Indiana 46805, USA
(Received 21 January 2008; published 8 September 2008)

We study chemical patterns arising from instabilities in reaction-diffusion-advection systems under the influence of shear flow. Turing pattern formation without shear flow can occur in an activator-inhibitor system as long as the diffusivity of the inhibitor is larger than the diffusivity of the activator. In the presence of shear flow, a homogeneous steady state can become unstable even if this condition is not satisfied. Chemical patterns arise as a result of this instability. We study this instability in a simple system consisting of two layers moving relative to each other. We carry out a linear stability analysis showing the onset of the instability as a function of the relative speed between the layers. We solve numerically the nonlinear reaction-diffusion-advection equations to obtain these patterns. We find stationary, oscillatory, and drifting patterns extending along each layer. We also find regions of bistability that allow the formation of localized structures. The instability is analyzed in terms of Taylor dispersion.

DOI: 10.1103/PhysRevE.78.036109 PACS number(s): 82.40.Ck, 47.54.−r

I. INTRODUCTION

Spatiotemporal chemical structures arising in controlled experiments, such as the ones observed in the Belousov-Zhabotinskii (BZ) reaction [1] or the chlorite–iodide–malonic acid (CIMA) reaction [2], can be explained by different mechanisms of pattern formation. Waves of chemical activity in the BZ reaction are caused by an excitable chemical system coupled to molecular diffusion [3,4]. The patterns in the CIMA reaction can be explained with a mechanism first proposed by Turing for biological morphogenesis [5]. This mechanism consists of two reacting chemicals with different molecular diffusivities, where one substance (the activator) increases its concentration due to a feedback process, while the other (the inhibitor) tends to diminish its concentration. Patterns arise if the diffusivity of the inhibitor is sufficiently larger than the diffusivity of the activator. This mechanism may also explain the formation of biological patterns [6].

The interaction between molecular diffusion, chemical reactions, and fluid flow results in other mechanisms of pattern formation. In the differential flow instability (DIFO) mechanism, two species flow with different velocities leading to an instability of the homogeneous, non-patterned state [7,8]. The flow-distributed oscillation (FDO) mechanism generates patterns as fresh chemicals are fed to a flowing oscillatory reaction [9,10]. Convective fluid motion induced by a propagating autocatalytic front results in axisymmetric and non-axisymmetric fronts in vertical tubes, fingering in Hele-Shaw cells, and convective vortices in larger containers. Shear flow can induce a chemical pattern in a reaction-diffusion-advection mechanism [11–13]. This shear-induced mechanism is different from the DIFO mechanism since both chemicals have the same fluid velocity, and it is different from the FDO mechanism since the chemical reaction is not oscillatory. The shear-induced mechanism also differs from the Turing mechanism since a pattern can form even if the diffusivity of the activator is larger than the diffusivity of the inhibitor. Previous studies for this instability consisted of a linear stability analysis of the homogeneous state under different conditions for shear flow. Evans [11] studied a simple system where a moving layer is coupled to a stationary layer, allowing for different species to diffuse across the layers, but not along the layers. Spiegel [12] used a linear velocity profile with a multiple-scale analysis to show a shear-induced instability. Coupling of Poiseuille flow to the Brusselator model showed that an instability can occur even if the conditions for Turing pattern formation are not met [13]. Numerical calculations using this model [13] showed stationary patterns in a reference frame comoving with the average velocity of the flow. Although these studies showed the instability mechanism, there is little work on the spatiotemporal structures arising from the instability. It is the purpose of this work to study such structures.

In this paper, we will study the formation of patterns due to shear flow using a two-layer system, where one of the layers moves relative to the other. Studies of Turing pattern formation in a two-layer model showed the existence of oscillatory patterns due to the coupling between the stationary layers [15,16]. Experiments in coupled layers showed patterns modulated by one another depending on the strength of the coupling [17]. In our model, we will use a reaction-diffusion system based on the Brusselator kinetics, allowing diffusion along each layer and across the layers [15]. The relative motion of the layers will provide the necessary shear to trigger an instability. Our analysis will not be limited only to the shear-induced instability, but will also include the effects of shear flow on Turing patterns. We will carry out a linear stability analysis of the homogeneous solution, showing the shear-induced instability in this system. Numerical

*Permanent address: Department of Physics, Indiana University Purdue University Fort Wayne, Fort Wayne, IN 46805.

solutions of the nonlinear equations will show different types of spatiotemporal behavior.

II. THE REACTION-DIFFUSION-ADVECTION EQUATIONS

Our system consists of two coupled layers in relative motion with one another. We describe the chemical reaction using the Brusselator model. This model was previously used to describe Turing patterns in coupled layers [15] and shear-flow instabilities in a Poiseuille flow [13]. Our equations consists of four coupled reaction-diffusion-advection equations:

$$\frac{\partial X_1}{\partial t} + \frac{V}{2}\frac{\partial X_1}{\partial x} = \frac{\partial^2 X_1}{\partial x^2} + \mu(X_2 - X_1) + f(X_1, Y_1), \tag{1}$$

$$\frac{\partial Y_1}{\partial t} + \frac{V}{2}\frac{\partial Y_1}{\partial x} = d\frac{\partial^2 Y_1}{\partial x^2} + d\mu(Y_2 - Y_1) + g(X_1, Y_1), \tag{2}$$

$$\frac{\partial X_2}{\partial t} - \frac{V}{2}\frac{\partial X_2}{\partial x} = \frac{\partial^2 X_2}{\partial x^2} + \mu(X_1 - X_2) + f(X_2, Y_2), \tag{3}$$

and

$$\frac{\partial Y_2}{\partial t} - \frac{V}{2}\frac{\partial Y_2}{\partial x} = d\frac{\partial^2 Y_2}{\partial x^2} + d\mu(Y_1 - Y_2) + g(X_2, Y_2). \tag{4}$$

Here X_i and Y_i represent the concentrations of chemicals X and Y, respectively, in the corresponding layer (labeled with the subindex i, either 1 or 2). The Brusselator model provides the reaction terms

$$f(X,Y) = A - (B+1)X + X^2 Y \tag{5}$$

and

$$g(X,Y) = BX - X^2 Y. \tag{6}$$

The layers move in opposite directions with a relative speed V as seen from the other layer, the parameter d is the ratio of the corresponding molecular diffusivities, while the parameter μ corresponds to the strength of coupling between the layers. We are interested in the effects of shear flow in a chemical system; therefore we will keep the parameters of the reaction terms constant through the analysis, setting the parameters $A=10$ and $B=100$. This choice of parameters provides a homogeneous steady state with $X_0=10$ and $Y_0=10$. Without shear motion and without coupling, each layer will undergo a Turing instability for $d>d_c=1.2345$. We will focus on the effects of the speed and coupling for different values of d.

We introduce perturbations to the steady state of the form $X_i=X_0+X_i' e^{\sigma t} e^{ikx}$ and $Y_i=Y_0+Y_i' e^{\sigma t} e^{ikx}$ arriving at a set of homogeneous equations for the amplitudes X_i' and Y_i':

$$\begin{bmatrix} F_k - iVk/2 & f_y & \mu & 0 \\ g_x & G_k - iVk/2 & 0 & d\mu \\ \mu & 0 & F_k + iVk/2 & f_y \\ 0 & d\mu & g_x & G_k + iVk/2 \end{bmatrix} \begin{bmatrix} X_1' \\ Y_1' \\ X_2' \\ Y_2' \end{bmatrix} = \begin{bmatrix} 0 \\ 0 \\ 0 \\ 0 \end{bmatrix}. \tag{7}$$

Here we define

$$F_k = f_x - k^2 - \mu - \sigma \quad \text{and} \quad G_k = g_y - dk^2 - d\mu - \sigma. \tag{8}$$

The corresponding partial derivates of the reaction functions f_x, f_y, g_x, and g_y are evaluated at the homogeneous steady state. We obtain the dispersion relation between the growth rate σ and the wave number k by requiring the determinant of the system to be zero. Equal diffusion coefficients ($d=1$) will result in a stable homogeneous state, since the diffusivity along the layers will simply lower the growth rate by k^2. The resulting system consists of shear flow and diffusivity only across the layers, which is stable for $d=1$ [11]. Therefore we study the cases that allow for pattern formation ($d \neq 1$). Our results for different values of the speed and interlayer diffusion will be presented in the next section.

We also carry out a numerical solution of full reaction-diffusion-advection equations. The space is discretized on a one-dimensional grid. The partial derivatives are approximated using finite differences on the grid. The time evolution is carried out using a forward simple Euler method, with a time step small enough to avoid numerical instabilities due to the advective and diffusive terms. These solutions provide a full spatiotemporal description of the system. In this work we limit ourselves to the study of the long-term behavior.

III. RESULTS

We carry out a linear stability analysis of the homogeneous steady solution of Eqs. (5) and (6) with $d=0.5$ as our diffusivity ratio. We set the value of the parameter μ to 25, unless otherwise noted. With this value the diffusivity of the inhibitor is smaller than the diffusivity of the activator; therefore the homogeneous state is stable for no fluid flow. This is illustrated in Fig. 1, where the curve corresponding to the real part of the growth rate [$\mathrm{Re}(\sigma)$] is always negative for fluid speed zero ($V=0$). In the same figure, we also display $\mathrm{Re}(\sigma)$ as a function of the wave number k for different values of the relative fluid velocity. All curves have a value of $\mathrm{Re}(\sigma)=-0.5$ for $k=0$, indicating the stability of the homogeneous state in the absence of diffusion. As we increase the value of V, there is still a local maximum at $k=0$, with a local maximum appearing away from $k=0$. Between the two maxima there is a cusplike minimum where the branch of the second highest eigenvalue overtakes the initially highest branch. At this point, there is more than one eigenvalue with the same real part. The maximum with $k \neq 0$ increases as the fluid speed increases. The maximum is positive at $V=25$, indicating an instability caused by the fluid flow. We also

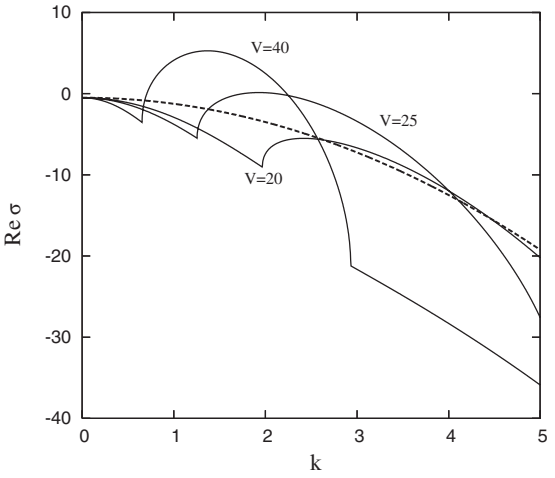

FIG. 1. Real part of the growth rate $[\mathrm{Re}(\sigma)]$ as a function of the wave number k for different layer velocities V. Here $d=0.5$ and $\mu=25$, resulting in a stable homogeneous steady state since $\mathrm{Re}(\sigma)<0$ for $V=0$ (dotted line). Larger fluid velocities V result in $\mathrm{Re}(\sigma)>0$.

notice that the wave number corresponding to the maximum real growth rate decreases as the velocity increases.

We test the results of the linear stability analysis by solving numerically the full reaction-diffusion-advection equations with small random perturbations of the homogeneous steady state as our initial conditions. For this choice of parameters, the linear stability analysis provides a critical velocity $V_c=24.9$, and a critical wavelength $\lambda_c=2\pi/k_c=3.25$. We chose a domain size equal to 40 spatial units to accommodate a number of critical wavelengths. We find that the perturbations died out for speeds less than 25.1, close to the result of the linear stability analysis on an unbounded medium. For speeds greater than 25.2, the system evolves into a steady patterned state. In Fig. 2 we display two patterns formed with this set of parameters but with different fluid velocities. In this figure, we show the spatial variation of the

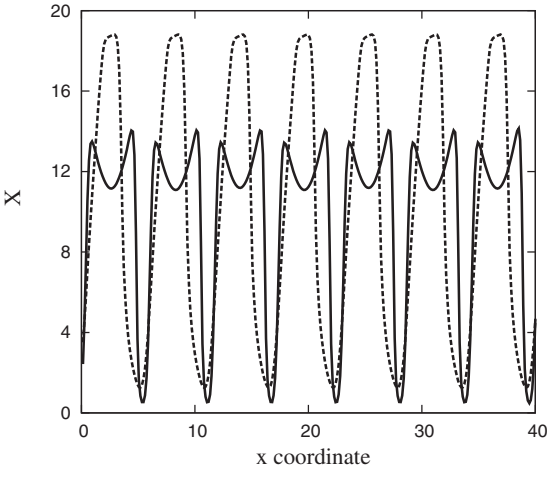

FIG. 2. Patterns formed by the shear-induced instability. We display the concentration of the variable X in one layer as a function of position x. The solid line corresponds to $V=18$. The dotted line corresponds to $V=55$. Here $d=0.5$ and $\mu=25$.

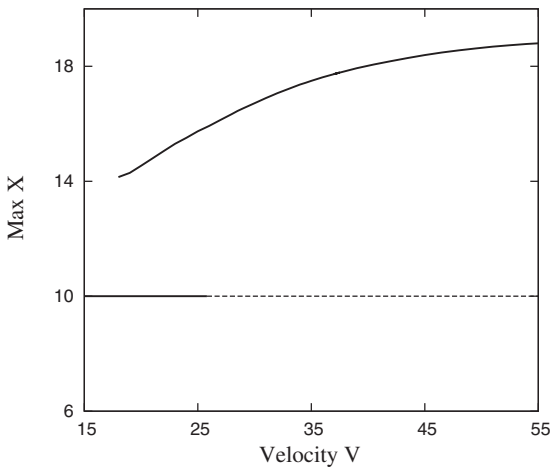

FIG. 3. Maximum concentration of the variable X for shear-induced patterns as a function of layer velocity V. The horizontal straight line at $X=10$ indicates the concentration for the homogeneous steady state. The solid lines indicate a stable state, where the dotted lines indicate an unstable state. There is a region of bistability between patterns and the homogeneous steady state. Here $d=0.5$ and $\mu=25$.

concentration X along one of the layers. The pattern formed with fluid velocity $V=55$ evolved from small perturbations to the homogeneous steady state as described above. The pattern consists of a peak intercalated by a concentration minimum. The other pattern displayed in Fig. 2, obtained with the same parameters but a fluid velocity of $V=18$, has two different peaks that are separated by a relative minimum and an absolute minimum. The fluid velocity for this pattern is much lower than the critical velocity V_c for the shear-induced instability calculated from the linear stability analysis. We obtained this pattern by slowly reducing the speed corresponding to the previous pattern. The pattern with two peaks appears for speeds below $V=46.0$. The presence of a relative minimum between two peaks resembles the "black-eye" structures observed in Turing patterns [14,15]. Therefore there is bistability between patterns and the homogeneous steady state. We study the bistable region by continuing the reduction of the fluid velocity as shown in Fig. 3. This figure displays the absolute maximum of the local concentration X as a function of the fluid velocity. Here we also display the value of the concentration X for the homogeneous steady state indicating its stability. We found that patterns formed with higher fluid velocities have a higher maximum. A region of bistability between the homogeneous steady state and the patterns occurs for fluid velocities below the critical velocity for the shear-induced instability. For values of fluid velocities below 17.2 we did not find a stable pattern.

The bistability between the patterns and the homogeneous steady state allows for the formation of localized structures as shown in Fig. 4. In this figure, we display the concentration X as a function of position showing localized structures surrounded by a homogeneous state. Each individual pattern forms by choosing different initial conditions for the reaction-diffusion-advection equations. Each initial condition corresponds to a spatial truncation of the extended pattern, filling the remainder of the space with the homogeneous so-

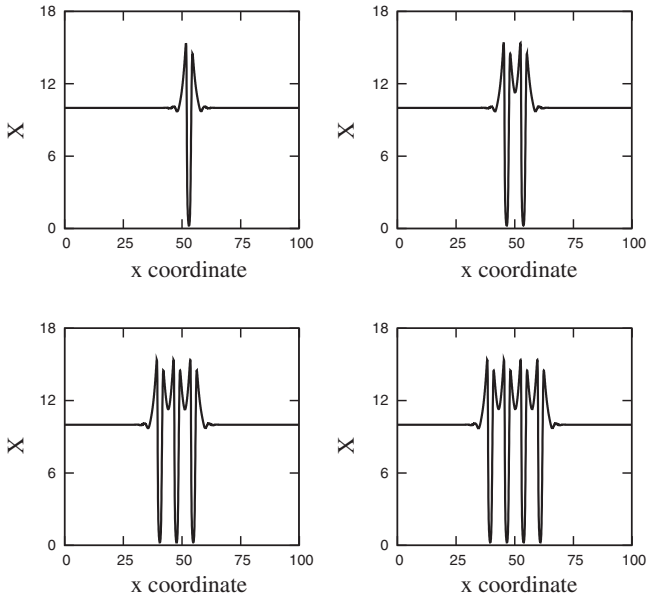

FIG. 4. Localized patterns formed by the shear flow instability. The four different steady patterns evolve from different initial conditions. Here $d=0.5$, $\mu=25$, and $V=24$.

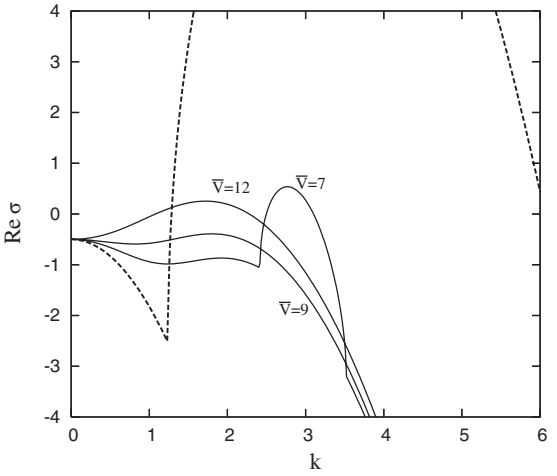

FIG. 5. Real part of the growth rate $[\mathrm{Re}(\sigma)]$ as a function of the wave number k for different layer velocities V. Here $d=1.65$ resulting in positive values for $\mathrm{Re}(\sigma)$ and $V=0$, indicating the instability of the homogeneous steady state (dotted line). For $V=9$, $\mathrm{Re}(\sigma)<0$, making the homogeneous steady state stable. For $V=12$, the maximum value of $\mathrm{Re}(\sigma)$ is positive, indicating an instability. Here the value of μ is set to 25.

lution. In this manner, we achieve patterns with a definite number of peaks and valleys. The smallest localized structure has only one minimum surrounded by two peaks of different height. Other structures present two to four absolute minima intercalated by a smaller relative minimum between them. The relative minimum is surrounded by two peaks of uneven height. The larger the size of the structure, the more it resembles the extended pattern. Localized structures, like the ones arising from the shear-induced instability, are also found sin other types of instabilities. Similar structures were observed in models of Turing pattern formation, such as the Brusselator model [18] or the more realistic chlorine dioxide–iodine–malonic acid model [19]. Experiments with the Belousov-Zhabotinskii reaction [20] also observed localized structures.

While shear flow induces an instability on a stable stationary reaction-diffusion state, its effect on an unstable state can either suppress or enhance the instability. In Fig. 5 we show the real part of the dispersion relation using the same set of parameters with the exception of $d=1.65$, which is larger than the critical value for the instability. This is shown in the curve for $V=0$, where there is a range of unstable wave numbers $[\mathrm{Re}(\sigma)>0]$. As we increase the speed of the shear flow $(V=7)$ the curve is lowered, reducing the range of unstable wave numbers. For a somewhat larger speed $(V=9)$, there is no unstable wave number, so the Turing instability disappears. However, for an even higher speed $(V=12)$, the real part of the growth rate once again takes positive values. In other words, the Turing instability is first washed out by the shear flow, making the homogeneous solution stable, and then again the system is destabilized by a higher fluid velocity. We show the effect on an already formed pattern in Fig. 6, where we compare two Turing patterns, one with fluid flow and the other without fluid flow. Here we chose the relatively low value of $V=7$ where the Turing instability is not suppressed, but its dispersion curve is diminished (Fig. 5). The pattern with advection has a wavelength close to the original Turing pattern but with a smaller amplitude. We also notice that, while the Turing pattern has peaks that are symmetric relative to the position of maximum concentration, the pattern with shear flow does not have this symmetry. Increasing the speed beyond $V=7.1$ takes us into the stable region. The homogeneous steady state remains stable for speeds up to $V=10.7$, where a new instability occurs.

Using the numerical solution to the equations, we find oscillatory patterns coexisting with the stable homogeneous state. In Fig. 7 we plot the concentration as a function of time for $V=7.5$ observing a pattern that resembles a standing wave. Each point of the space oscillates with a set amplitude,

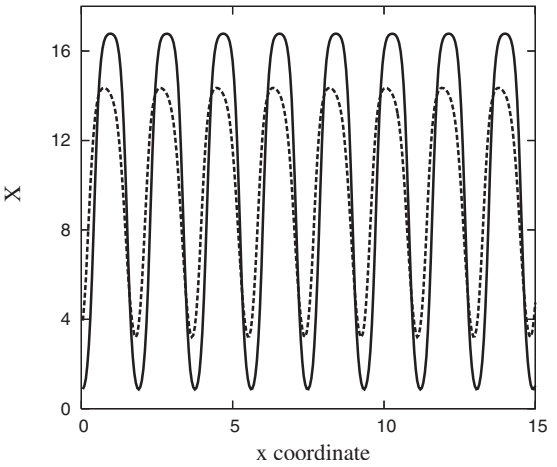

FIG. 6. Concentration of the variable X in one layer as a function of position x. The solid line indicates a Turing pattern formed by the reaction-diffusion mechanism alone $(V=0)$. The dotted line corresponds to the same pattern with shear flow $(V=7)$. Here $d=0.5$ and $\mu=25$.

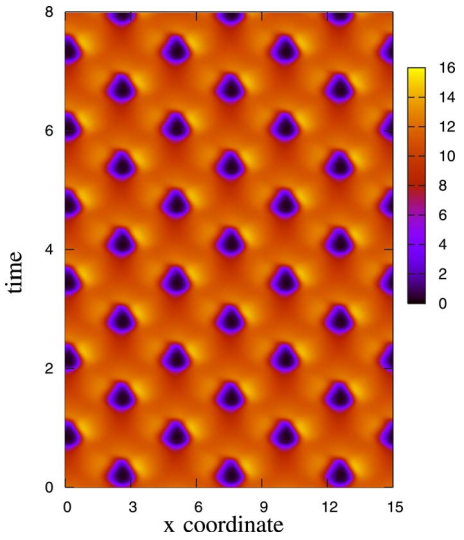

FIG. 7. (Color online) An oscillatory pattern induced by shear flow ($d=0.5$, $\mu=25$, and $V=7.0$). The pattern resembles a standing wave.

without changing its position. Each oscillatory segment repeats itself after a certain spatial distance. This pattern was obtained starting with a Turing pattern and gradually increasing the fluid velocity. Increasing the fluid speed to $V=8.0$ leads to oscillations that are no longer localized. Figure 8 shows a pattern similar to the one in Fig. 7 but where the oscillations are no longer localized. There is a drift of the oscillatory region to the left. We also obtained the same pattern drifting to the right using different initial conditions. This is consistent with the fact that the equations do not have a preferred direction, since both layers move with the same speed but in opposite directions.

The disappearance of the Turing pattern with increasing fluid flow, and the consequent reappearance of an instability, depends also on the strength of the coupling between the two

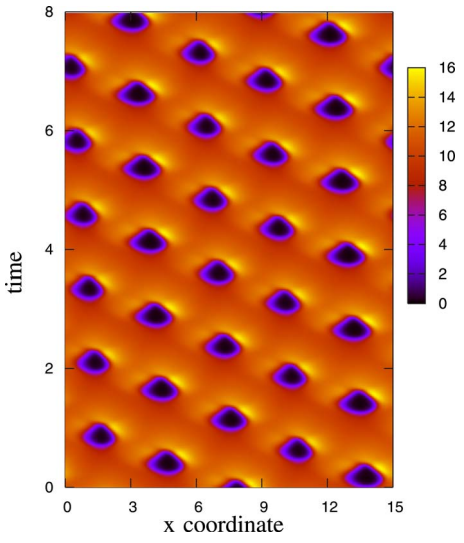

FIG. 8. (Color online) An oscillatory pattern induced by shear flow ($d=0.5$, $\mu=25$, and $V=8.0$). The pattern resembles a standing wave slowly drifting to the left.

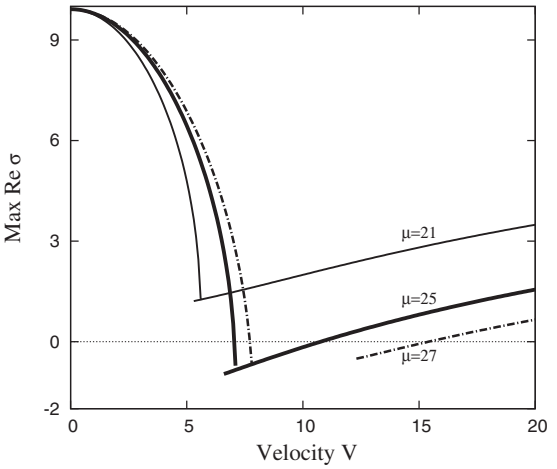

FIG. 9. Maximum value of Re(σ) as a function of layer velocity V. Here we chose $d=1.65$; consequently there is a Turing instability at $V=0$. For layer coupling $\mu=21$, the maximum Re(σ) is always positive, indicating that the homogeneous steady state is always unstable. For $\mu=25$ and 27, there is a range of velocities where the maximum Re(σ) is negative, indicating that the homogeneous steady state is stable.

layers as represented by the diffusivity parameter μ. In Fig. 9 we show the relative maximums of the dispersion relations [Re(σ)] as a function of the velocity for different values of μ. For $V=0$ we find that the maximum growth rate is 9.9 corresponding to the Turing instability. As the velocity begins to increase, this maximum decreases for the values of μ studied in Fig. 9 ($\mu=21$, 25, and 27). The case for $\mu=25$ was the one we studied in Fig. 5, where we display the full dispersion curves, showing a transition from Turing instability to a stable homogeneous state. This is shown in Fig. 9, where we display the maximum real part of the growth rate decreasing and becoming negative with increasing speed. We also notice that as we increase the speed a secondary relative maximum appears; this maximum eventually becomes larger, while the original maximum disappears. The existence of two maximums in the dispersion relation can be observed in Fig. 5, where the curve for $V=7$ contains two relative maximums, one of them positive. We can also notice in Fig. 5, that the curve corresponding to $V=9$ has only one maximum with negative value. Increasing to $V=12$, the maximum is now positive, signaling a new instability. The presence of the two maxima in the dispersion relation (Fig. 5) is indicated in Fig. 9 by two different curves for each value of μ, one of the curves monotonically decreases from a maximum at $V=0$, while the other increases from the point where the second maximum appears. While the curves for $\mu=25$ descend to negative growth rates, the curves for $\mu=21$ always remain positive, indicating that there is always an instability regardless of the value of V. In this case the diffusive coupling between the layers is too small to result in the disappearance of the instability. For $\mu=27$ there is a larger range of speeds where the homogeneous state is stable compared to the results for $\mu=25$. In this case ($\mu=27$), there is also a range of velocities where the dispersion relation has no relative maximum, the dispersion relation monotonically decreases from Re(σ)=0, with all values of the real part of the growth rate

being negative. Increasing the flow speed leads to a new maximum in the dispersion curve. This maximum appears once the speed reaches the value of $V=12.3$. At this speed the maximum is negative, therefore all growth rates are negative, but for speeds greater than 15.3 the maximum becomes positive indicating instability. This instability has a nonzero imaginary part of the growth rate near the threshold indicating the possibility of a convective or oscillatory instability. Close to the initial Turing instability, the imaginary part of the growth rate is zero.

The shear-induced instability can be understood in terms of Taylor dispersion. Taylor dispersion provides an effective diffusion coefficient for diffusive concentrations in a shear flow. Taylor's original work involved fluid flowing in a cylindrical pipe of radius a under Poiseuille flow conditions [21]. The effective diffusivity approximation is valid once there is enough diffusion across the pipe, this corresponds to a time significantly larger than a^2/D. For two layers moving relative to one another the corresponding effective diffusivity is equal to $D_{\text{eff}}=D+V^2/(8\mu)$, valid after a time of the order $1/\mu$ where enough interlayer diffusion has taken place [22]. Applying this to the ratio of diffusivities between the inhibitor $(D_v=d)$ and the activator $(D_u=1)$ we find

$$d_{\text{eff}} = \frac{d + V^2/(8d\mu)}{1 + V^2/(8\mu)}$$

which for large speeds gives $d_{\text{eff}} \approx 1/d$. That is, for sufficiently high speeds the ratio between the diffusivities can be reversed. The Turing instability is triggered when the diffusivity ratio d is larger than a critical value $d_c>1$. We can accomplish this with an effective diffusivity using a sufficiently large speed. We can begin with a homogeneous steady state that is stable at zero relative velocity, where the diffusivity of the activator is larger than the diffusivity of the inhibitor $(d<1)$, then increase the velocities to obtain an effective diffusivity greater than 1, eventually becoming greater than the critical diffusivity d_c for Turing pattern formation. Taylor dispersion can provide the instability mechanism, contrary to what was found with the approximations of Ref. [12], where the Taylor dispersion term led to a stabilizing mechanism.

Taylor dispersion also helps us to understand how a homogeneous steady state with a Turing instability can become stable under shear flow. If the diffusivity ratio d is larger than the critical value, increasing the fluid velocity will tend to diminish Taylor's effective diffusivity below the critical value, eventually making it $1/d$, which is less than 1. Using the formula for the effective diffusivity, the initial diffusion coefficients, and the critical value d_c for Turing instability, we can calculate the velocity required for the effective diffusivity to be equal to the critical value for Turing pattern formation. In Fig. 10 we show these results and compare them with the ones obtained with the two-layer model. In this figure, we find the critical velocity for an instability for different values of the original ratio d. For $d<1$, both methods provide a critical speed for a shear-induced instability. However, with a very small diffusivity ratio, Taylor dispersion gives a critical velocity close to zero, while the full solution requires a much larger value. For larger diffusivity ratios but still $d<1$, the results are closer to each other. In both cases there is a threshold for d, where no velocity will trigger an instability. In the case of Taylor dispersion the threshold corresponds to $1/d_c$, the asymptotic value of d_{eff}. For diffusivity ratios $d>1$ and relative velocity $V=0$, we find the Turing instability if the ratio d is greater than the critical ratio d_c. Increasing the speed of the layers will reduce the effective diffusivity, eventually lowering it below the critical diffusivity ratio, stabilizing the originally unstable state. This is shown in Fig. 10 where small velocities increase the ratio d required for a Turing instability, for both the results based on Taylor dispersion approximation and the results based on the full solution. However, as we increase the velocity, the Taylor dispersion results keep increasing the value of d for the instability, while the full solutions deviate completely from this trend. As we increase the velocity, a new instability appears that cannot be described by Taylor dispersion. According to Taylor dispersion, for every $d>1$ there is a velocity that makes the system stable. For the full solutions, unstable states with d greater than 1.8 cannot be stabilized by shear flow. For values of d slightly below 1.8 the system can be stabilized, but an instability reappears as the speed is further increased. For unstable states with d slightly above d_c the instability disappears and will not reappear.

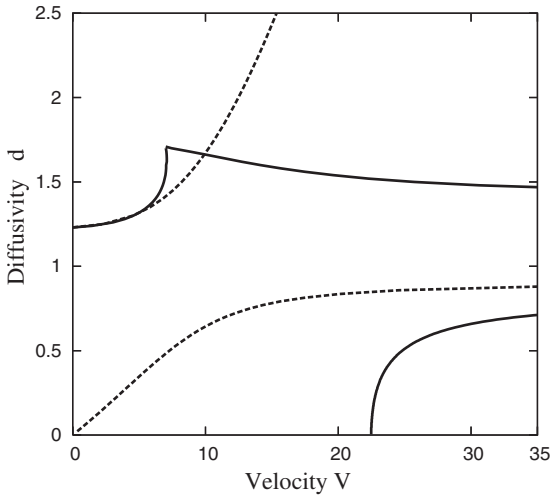

FIG. 10. Critical diffusivity ratio for instability of the homogeneous steady state as a function of layer velocity V. The solid lines correspond to results from the linear stability analysis. The dotted lines correspond to modifying the diffusion coefficients using the Taylor dispersion limit. Here the parameter μ is set to 25.

IV. EXPERIMENTAL APPLICATIONS

The theoretical Brusselator model is useful to understand pattern formation in reaction-diffusion systems, although it is not derived from a specific chemical reaction. However, we can estimate the dimensional values of the parameters μ and the relative velocity V by using the diffusivity of 2.0×10^{-5} cm^2/s and a wavelength of 0.3 mm typical of Turing patterns. This can be achieved by multiplying the reaction terms by a dimensioned constant $\gamma=0.35$ 1/s while consid-

ering Turing patterns at the diffusivity threshold $d_c=1.2345$. In this way we obtained a dimensioned coupling constant $\mu\gamma$ and a dimensioned velocity $V\sqrt{D\gamma}$ making our typical velocities of the order of 0.6 mm/s. Experiments to obtain shear-induced patterns can be carried out in cylindrical tubes, where the correction for the Taylor dispersion diffusivity is given by $a^2V^2/48D$, where a is the tube radius. Using this correction and matching it to the correction in the two-layer system $[V^2/(8\mu)]$ results in tubes of diameter around 0.2 mm, which can be achieved in microfluidic systems. Studies in larger-diameter tubes will require new calculations that will match not only the parameter μ, but also the correct tube geometry.

V. CONCLUSIONS

We have shown that shear flow can induce chemical instabilities in a two-layer model. This instability can occur even if conditions for Turing instability are not satisfied, namely, if the diffusivity of the activator is larger than the diffusivity of the inhibitor. This behavior can be understood in terms of the ratio of effective diffusivities due to Taylor dispersion. If the diffusivity ratio between the inhibitor and the activator is less than 1, the effective diffusivity ratio increases with increasing layer velocity, allowing it to increase beyond the critical diffusivity ratio for Turing pattern formation. In a system with an initial Turing instability, a slow shear flow tends to suppress the formation of a Turing pattern. In this case, Taylor dispersion reduces the effective diffusivity ratio, thus inhibiting Turing pattern formation. However, for faster shear flow our results show that the homogeneous steady state is unstable. This result cannot be explained by the Taylor dispersion approximation, since in this case Taylor dispersion always reduces the effective diffusivity ratio. Our numerical solutions of the reaction-diffusion equations led to several spatiotemporal patterns, such as steady patterns of fixed wavelength. We found regions of bistability that allow the formation of oscillatory patterns, as well as localized patterns confined inside a homogeneous steady state. Since experiments in chemical pattern formation take place in liquids or porous media such as gels, experiments can be designed to test the effects of shear flow.

ACKNOWLEDGMENT

This work was supported by an award from Research Corporation.

[1] A. T. Winfree, Science **175**, 634 (1972).
[2] V. Castets, E. Dulos, J. Boissonade, and P. De Kepper, Phys. Rev. Lett. **64**, 2953 (1990).
[3] J. P. Keener and J. J. Tyson, Physica D **21**, 307 (1986).
[4] J. J. Tyson and J. P. Keener, Physica D **32**, 327 (1988).
[5] A. Turing, Philos. Trans. R. Soc. London, Ser. B **327**, 37 (1952).
[6] S. Sick, S. Reinker, J. Timmer, and T. Schlake, Science **314**, 1447 (2006).
[7] A. B. Rovinsky and M. Menzinger, Phys. Rev. Lett. **69**, 1193 (1992).
[8] A. B. Rovinsky and M. Menzinger, Phys. Rev. Lett. **70**, 778 (1993).
[9] M. Kaern and M. Menzinger, Phys. Rev. E **60**, R3471 (1999).
[10] P. N. McGraw and M. Menzinger, Phys. Rev. E **68**, 066122 (2003).
[11] G. T. Evans, J. Theor. Biol. **87**, 297 (1980).
[12] E. A. Spiegel and S. Zaleski, Phys. Lett. **106A**, 335 (1984).
[13] D. A. Vasquez, Phys. Rev. Lett. **93**, 104501 (2004).
[14] G. H. Gunaratne, Q. Ouyang, and H. L. Swinney, Phys. Rev. E **50**, 2802 (1994).
[15] L. Yang, M. Dolnik, A. M. Zhabotinsky, and I. R. Epstein, Phys. Rev. Lett. **88**, 208303 (2002).
[16] L. Yang and I. R. Epstein, Phys. Rev. Lett. **90**, 178303 (2003).
[17] I. G. Berenstein, M. Dolnik, L. Yang, A. M. Zhabotinsky, and I. R. Epstein, Phys. Rev. E **70**, 046219 (2004).
[18] O. Jensen, V. O. Pannbacker, E. Mosekilde, G. Dewel, and P. Borckmans, Phys. Rev. E **50**, 736 (1994).
[19] O. Jensen, V. O. Pannbacker, G. Dewel, and P. Borkmans, Phys. Lett. A **179**, 99 (1993).
[20] V. K. Vanag and I. R. Epstein, Phys. Rev. Lett. **92**, 128301 (2004).
[21] G. I. Taylor, Proc. R. Soc. London, Ser. A **253**, 67 (1953).
[22] W. C. Thacker, J. Phys. Oceanogr. **6**, 66 (1976).